Tunable synthesis of (Mg–Ni)-based hydrides nanoconfined in templated carbon studied by in situ synchrotron diffraction

Claudia Livia Zlotea, Fermin Cuevas, Jérome Andrieux, Camelia Matei Ghimbeu, Eric M. Leroy, Eric Leonel, Stephane Sengmany, Cathie Vix-Guterl, Roger Gadiou, Thierry Martens, et al.

Tuned synthesis of (Mg-Ni)-based hydrides nanoconfined in templated carbon studied by *in situ* synchrotron diffraction

Claudia Zlotea[1]*, *Fermin Cuevas*[1], *Jerome Andrieux*[2], *Camelia Matei-Ghimbeu*[3], *Eric Leroy*[1], *Eric Leonel*[1], *Stephane Sengmany*[1], *Cathie Vix-Guterl*[3], *Roger Gadiou*[3], *Thierry Martens*[1] *and Michel Latroche*[1]

[1] Institut de Chimie et des Materiaux de Paris Est, UMR 7182, CNRS-UPEC, Thiais, France

[2] ESRF, Grenoble, France

[3] Institut de Sciences des Matériaux de Mulhouse, LRC 7227, CNRS, Mulhouse, France

claudia.zlotea@icmpe.cnrs.fr

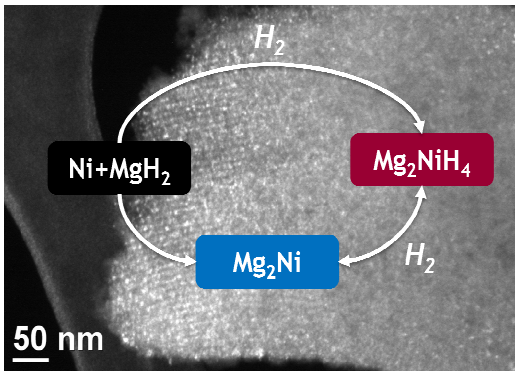

ABSTRACT

The formation of ultra-small Mg-based particles nanoconfined into the mesopores of a carbon template was studied by *in situ* synchrotron diffraction. Either Mg_2Ni or Mg_2NiH_4 nanoparticles can be directly formed starting from separate Ni and MgH_2 species by tuning the H_2 pressure. Both ultra-small Mg_2Ni and Mg_2NiH_4 nanoparticles (~4 nm) are extremely stable against coalescence during hydrogen sorption cycling and prolonged exposure to high temperature as compared to Mg and MgH_2 nanoparticles that show severe coalescence under same experimental conditions. The structural transition reported in bulk Mg_2NiH_4 from high temperature cubic to low temperature monoclinic structure is no longer observed for the nanoconfined particles. Hydrogen absorption/desorption in nanosized Mg_2Ni is reversible and desorption kinetics from Mg_2NiH_4 proceeds very quickly (~5 min) even at 483 K. On the contrary, the thermodynamics properties are not altered by nanoconfinement. This study opens new routes for successful nanoconfinement of stoichiometric hydrides into the pores of carbon hosts along with a better understanding of nanochemistry.

KEYWORDS: nanoconfinement, hydrogen storage, complex metal hydride, size effect, synchrotron X-ray diffraction

1. Introduction

Downsizing and nanoconfinement are very attractive strategies for improving the hydrogen sorption properties of metal hydrides.[1,2] Among them, MgH_2 has many advantages as hydrogen storage material. Mg is a cheap and abundant metal that offers high specific (7.6 wt.% H) and volumetric (109 $g_H \cdot L^{-1}$) hydrogen storage capacities.[3] However, the main drawbacks of MgH_2 are slow kinetics of hydrogen sorption and high thermodynamic stability. Nanoconfinement holds promise to adjust thermodynamics, improve kinetics and reversibility of hydrogen sorption.[4-8] At the nanoscale, the thermodynamic stability of hydrides is significantly influenced by the surface energy.[1] Kinetics of sorption can be improved by shorter hydrogen diffusion paths in nanosized hydrides. Indeed, the desorption kinetics of nanosized

MgH_2 were reported to be much faster and the desorption temperature lower than bulk hydride.[6,8] Thermodynamic changes of MgH_2 due to nanoconfinement have recently been claimed.[9] Furthermore, nanoconfinement can offer an interesting approach to stabilize nanoparticles against coalescence during exposure to high temperature and hydrogen absorption/desorption cycling.

Although hydrogen sorption properties of MgH_2 embedded into different carbon scaffolds have been largely reported,[4-7] very scarce studies have been done on nanoconfined Mg-based intermetallics. A previous publication detailed favorable hydrogen desorption properties for $Mg_{1-x}Ni_xH_y$ nanocrystals supported in carbon.[10] The samples were prepared by Mg melt infiltration in graphitic carbon (500 m^2 g^{-1}) onto which Ni nanoparticles have been first deposited. The samples were multiphased and showed complex desorption behaviors. Undoubtedly, the preparation of nanoconfined Mg-3*d* metal-H_x complex hydrides (Mg_2NiH_4, Mg_2CoH_5 or Mg_2FeH_6) directly into nanopores of supporting host is a very challenging synthetic work that might explain the limited number of publications on this subject.

The objective of this work is to investigate new synthetic routes to form complex Mg_2NiH_4 hydride directly in the pores of a templated carbon host from nanoscaled Ni and MgH_2. The hydrogen sorption properties of nanoconfined Mg_2NiH_4 hydride were determined by *in situ* and *ex situ* characterization techniques. To our knowledge, this is the first reported work on nanoconfined Mg_2NiH_4 where kinetics, thermodynamics and reversibility data were obtained.

2. Experimental details

a. Hybrid synthesis

The hybrid material was prepared following three steps: carbon template (CT) is produced first by nanocasting, Ni nanoparticles are then preformed into CT's porosity and finally MgH_2 nanoparticles are added into the pores of Ni-containing CT. The as-synthesized hybrid consists of a dispersion of both Ni and MgH_2 nanoparticles embedded within the pores of CT.

The mesoporous CT was obtained by a replica method of the SBA-15 silica. Synthesis details of SBA-15, mesoporous CT and corresponding textural properties are given elsewhere [11-13]. The CT displays a

hexagonal arrangement of carbon tubes with a very well organized mesoporosity of 3-4 nm. The synthesis of Ni nanoparticles was performed by an incipient wetness method.[14] The CT in powder form was impregnated with a solution of $Ni(NO_3)_2 \cdot 6H_2O$ dissolved in pure water and the mix was stirred for several hours followed by drying in air at 340 K overnight. The metal ions were reduced by heating the dried powder in a Ar/H_2 flow (0.5 $L \cdot min^{-1}$) at 573 K for 3 hours. The sample was degassed under secondary vacuum and further manipulated without air exposure. The last step of the synthesis is the formation of MgH_2 nanoparticles by impregnation with an organometallic precursor (Bu_2Mg in heptane 1.0 M commercially available from Sigma Aldrich) followed by hydrogenation (5 MPa, 423 K). This synthesis step was described in detail elsewhere.[15]

b. Characterization

The chemical composition of the as-synthesized hybrid was determined by inductively coupled plasma optical emission spectroscopy (ICP-OES). Besides the carbon host (80 wt.%), it contains 13.2 wt.% Mg and 6.8 wt.% Ni, respectively, corresponding to the $Mg_{4.6}Ni$ stoichiometry. This composition is higher than 2:1 that corresponds to our synthetic objective (Mg_2NiH_4). An excess of Mg has been used to directly compare the behavior of pairs of nano-species (Mg/MgH_2 and Mg_2Ni/Mg_2NiH_4) within the pores of the same hybrid material under identical experimental conditions. Moreover, small Mg loss may also occur by inevitable oxidation.

Microstructural analyses were performed by *ex situ* Transmission Electron Microscopy (TEM-Tecnai F20 with a Field Emission Gun 200 kV, punctual resolution 0.24 nm and Energy Filtering GIF). A special Gatan air-tight sample holder was used for sample preparation inside a glove box and sample transfer. The sample holder was cooled down to 110 K to avoid sample decomposition by beam irradiation in the microscope. The analysis of several TEM images allowed a statistical calculation of the average particle size.

In situ synchrotron X-ray diffraction (XRD) experiments have been undertaken on the ID15b beam line at ESRF in Grenoble (France). A monochromatic mode at an energy of 90 keV and a pixium area detector have been used allowing high brilliance, short wavelength (0.14239 Å) and very fast recording

of XRD patterns. A specially designed high pressure and high temperature device was used as sample environment allowing controlled heating under hydrogen pressure. Rietveld refinements of XRD patterns have been done using the FullProf program to determine the crystalline parameters and the phase evolution as function of temperature/hydrogen pressure or time. The average crystallite size of different phases was determined from the Lorentzian component of the "Thompson-Cox-Hastings pseudo-Voigt" profile shape function, as described eleswhere.[16]

The hydrogen desorption properties have been studied by thermal desorption spectroscopy (TDS) using a homemade instrument detailed in a previous report.[15] The sample was loaded without air exposure and the H_2 partial pressure was recorded while applying a constant temperature rate of 10 $K \cdot min^{-1}$ from 300 to 700-750 K.

Differential scanning calorimetric (DSC) experiments have been performed under hydrogen atmosphere with the help of a Setaram Sensys Evo instrument equipped with a high accuracy 3D Calvet sensor. The sample was loaded without air exposure and a constant temperature ramp of 5 $K \cdot min^{-1}$ from 300 to 673 K was applied.

3. Results

A HAADF-STEM image of the as-synthesized sample is shown in Figure 1. It shows both Ni and MgH_2 crystalline nanoparticles homogeneously dispersed into the porosity of the CT (XRD pattern at the bottom of Figure 2). Clear identification of Ni and MgH_2 nanoparticles is not possible from the STEM image. The nanoparticles sizes span between 2 and 11 nm, irrespective to their nature.

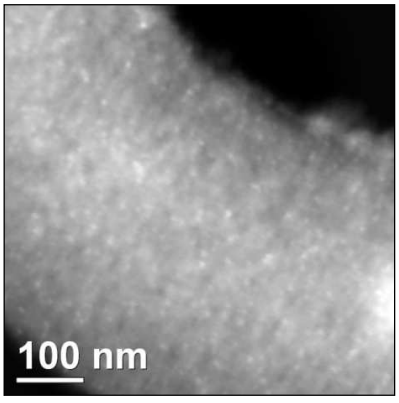

Figure 1. HAADF-STEM image of the as-synthesized sample.

Four *in situ* synchrotron XRD experiments have been performed under different temperature and hydrogen pressure conditions. The first two studies have been done starting from the as-synthesized hybrid whereas the last two from the hydrogenated sample (523 K and 0.57 MPa H_2).

(1) the as-synthesized hybrid was studied under 0.56 MPa H_2 pressure with a constant heating ramp of 2 $K \cdot min^{-1}$,

(2) another portion of the as-synthesized hybrid was measured under 2 MPa H_2 pressure with a constant heating ramp of 2 $K \cdot min^{-1}$,

(3) the hydrogenated sample was studied during a desorption pressure-composition-isotherm at 523 K in the pressure range from 0.57 down to 0.01 MPa,

(4) the hydrogenated sample was followed during isothermal dehydrogenation/hydrogenation cycling at 523 K and 483 K.

Evolution of the diffraction patterns during the first experiment are shown in figure 2 (left). The corresponding phase variations *versus* temperature, as determined from Rietveld refinements, are plotted (Figure 2 – right). The CT shows very broad peaks due to its weak crystalline organization. The diffraction peaks from CT and Ni overlap forming a broad peak at $2\theta \sim 4°$. Close to 570 K the width of this peak enlarges. This has been accounted by Mg oxidation that is unfortunately unavoidable under our experimental conditions. However, the intensity of this peak remains stable showing that no more oxidation process occurs afterward.

Both Ni (cubic $Fm\bar{3}m$; a = 3.54 ± 0.01 Å at 350 K) and MgH_2 (tetragonal $P4_2/mnm$; a = 4.518 ± 0.007 Å, c = 3.019 ± 0.007 Å at 350 K) crystalline phases are present in the sample at 350 K, with 29 and 71 wt.% for Ni and MgH_2, respectively. The percentage values are obtained neglecting the CT contribution to the diffraction patterns and are in good agreement with the ICP-OES result. The average crystallite sizes of Ni and MgH_2 phases are 3 and 8 nm, respectively.

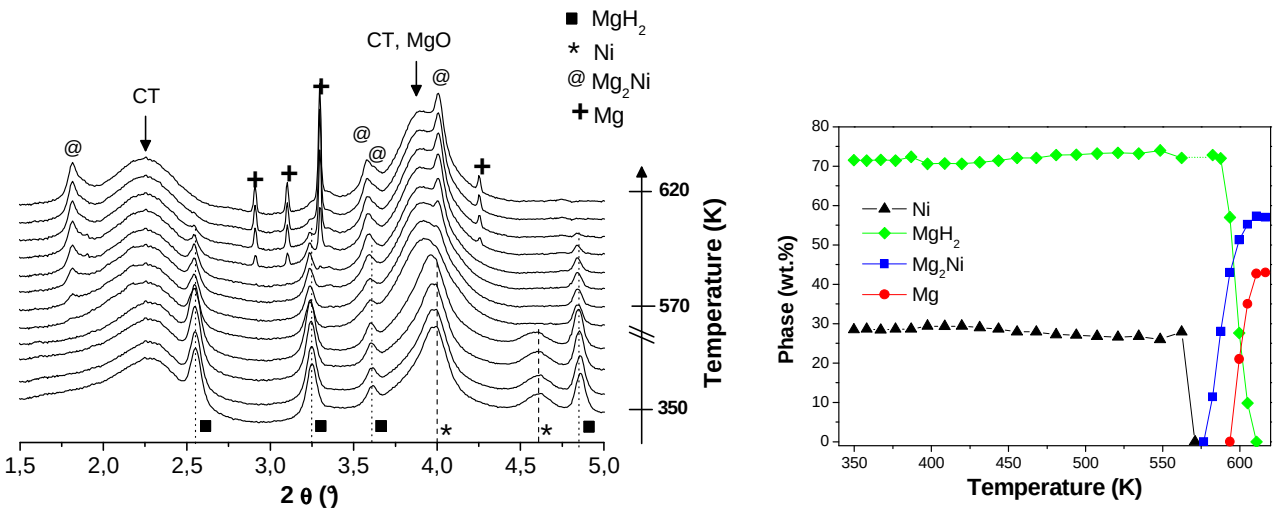

Figure 2. *In situ* XRD pattern evolution of as-synthesized hybrid (left) and corresponding phase variations (right) during heating from 350 to 620 K with 2 K·min^{-1} under 0.56 MPa of H_2.

Ni amount slightly decreases with temperature from 350 to 550 K and then completely vanishes between 550 and 570 K. Above this temperature the phase Mg_2Ni (hexagonal $P6_222$ a; a = 4.266 ± 0.013 Å, c = 13.46 ± 0.06 Å at 600 K) forms and its amount constantly increases with temperature before stabilizing beyond 610 K (Figure 2 – right). At the same time, the MgH_2 phase starts to decrease at 590 K and completely disappears at 610 K. Pure Mg is formed by hydrogen desorption from MgH_2 above 600 K. At 620 K, beside the CT phase, the sample contains 57 and 43 wt.% of Mg_2Ni and Mg crystalline phases and the average crystallite sizes are 10 and 200 nm, respectively.

The second *in situ* XRD experiment was done starting from another portion of the as-synthesized sample under higher hydrogen pressure: 2 MPa (Figure 3 – left). A constant temperature ramp of 2 K·min^{-1} from 300 to 660 K was applied. The corresponding phase variations are shown in Figure 3 (right).

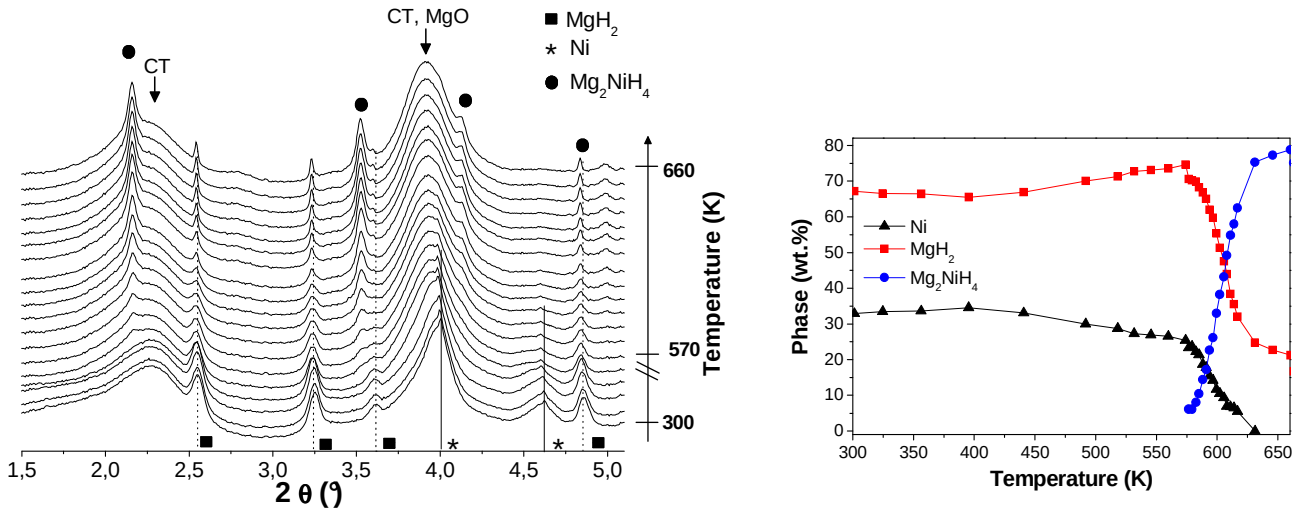

Figure 3. *In situ* XRD patterns of as-synthesized hybrid (left) and corresponding phase evolution (right) during heating from 300 to 660 K with 2 K·min^{-1} under 2 MPa H_2.

The Ni amount is almost constant between 300 and 450 K followed by a slight decrease up to 570 K. At this temperature, the hydride phase Mg_2NiH_4 (cubic $Fm\bar{3}m$; a = 6.52 ± 0.05 Å at 570 K) forms and its amount significantly increases with temperature at the expense of both Ni and MgH_2 phases. At 630 K, Ni completely disappears whereas MgH_2 stabilizes at 21 wt.%. The phase Mg_2NiH_4 represents 79 wt.% at 660 K.

The average crystallite sizes of Mg_2NiH_4 and MgH_2 hydride phases have been derived from the line widths and their thermal variations are shown in Figure 4.

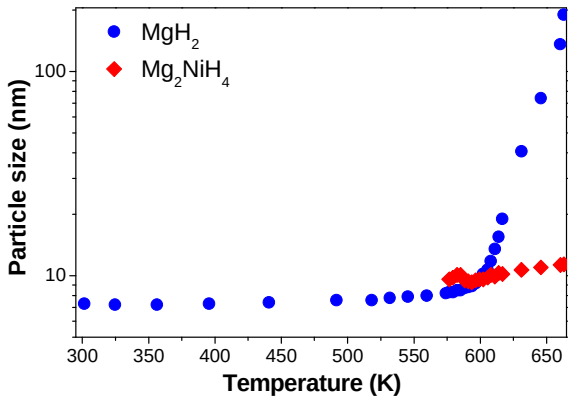

Figure 4. Thermal variation of the average crystallite sizes of Mg_2NiH_4 and MgH_2 during heating with 2 K·min^{-1} from 300 to 660 K under 2 MPa of H_2.

The average size of Mg_2NiH_4 nanoparticles is constant around 10 nm over the whole domain of existence (570 – 660 K), while the average size of MgH_2 drastically grows from 8 nm at 570 K to 200 nm at 660 K.

Previous to the third and forth *in situ* XRD measurements, the hybrid was hydrogenated as follows: firstly, the Mg_2Ni and Mg phases were formed at 523 K and low H_2 pressure (0.04 MPa). Secondly, these phases were hydrogenated under 0.57 MPa H_2 pressure at 523 K. The hydrogenated hybrid contains Mg_2NiH_4 and MgH_2 crystalline phases.

During the third *in situ* XRD measurement, a desorption pressure-composition-isotherm was performed step by step at constant temperature (523 K) in the pressure range from 0.57 to 0.01 MPa on the hydrogenated hybrid (Figure 5 – left). From the XRD pattern analysis, the desorption PCT curve could be calculated giving the equilibrium pressure *versus* the hydrogen content (H/M) in Mg_2NiH_4 (Figure 5 – right). All data points are collected at equilibrium pressure.

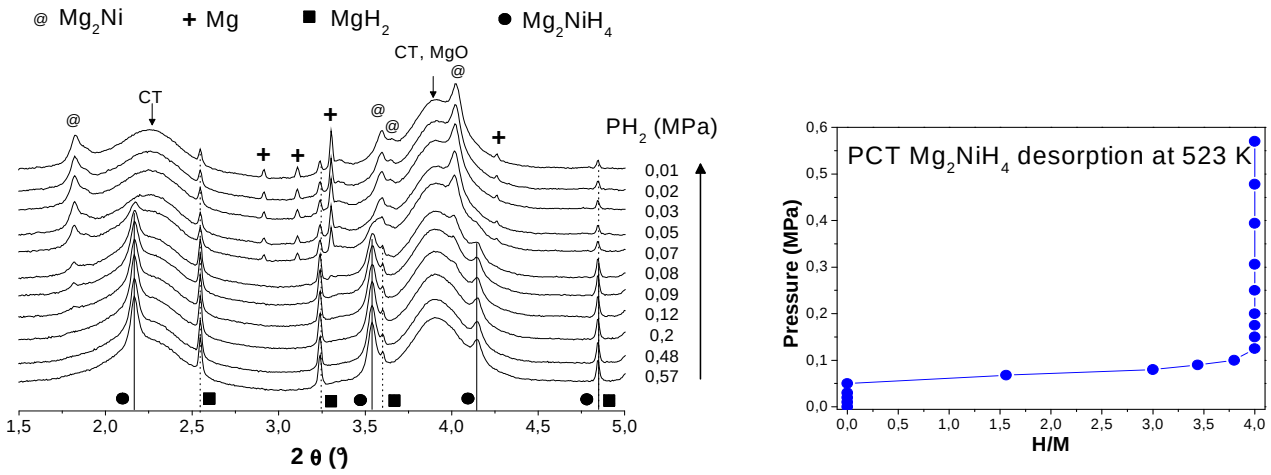

Figure 5. *In situ* XRD patterns collected during the PCT desorption at 523 K on the hydrogenated hybrid (left) and calculated desorption PCT for nanosized Mg_2NiH_4 (right).

When decreasing the pressure from 0.57 down to 0.2 MPa, no hydrogen desorption occurs for Mg_2NiH_4 and MgH_2 (Figure 5 – left). However, in the pressure range 0.12 – 0.07 MPa, Mg_2NiH_4 starts to desorb hydrogen forming Mg_2Ni (Figure 5 – right). The Mg_2NiH_4 phase completely transforms into Mg_2Ni at 0.05 MPa H_2 pressure. For MgH_2, the hydrogen desorption occurs only below 0.07 MPa. Finally, at 0.01

MPa, the crystalline phases are Mg_2Ni, Mg and some remaining MgH_2 (the kinetics of desorption are too slow at this temperature to fully desorb this hydride). The desorption plateau pressure for Mg_2NiH_4 is rather sloppy and is comprised between 0.1 and 0.07 MPa at 523 K.

The fourth *in situ* synchrotron XRD experiment studies the isothermal cycling behavior of the hydrogenated hybrid. The hydrogenation was realized as described previously. Four desorption/absorption cycles were performed by switching the hydrogen pressure between 0.03 and 0.57 MPa at 523 K followed by two cycles at 483 K (Figure 6). The absorption/desorption in Mg_2Ni is completely reversible under these conditions, whatever the temperature. The sample was finally cooled down to 300 K under 0.57 MPa. At this temperature, the crystalline phases observed (top pattern in Figure 6) are Mg_2NiH_4 and MgH_2. Small traces of pure Mg could be as well noticed. Mg_2NiH_4 retains the high temperature cubic crystalline structure (cubic $Fm\bar{3}m$).

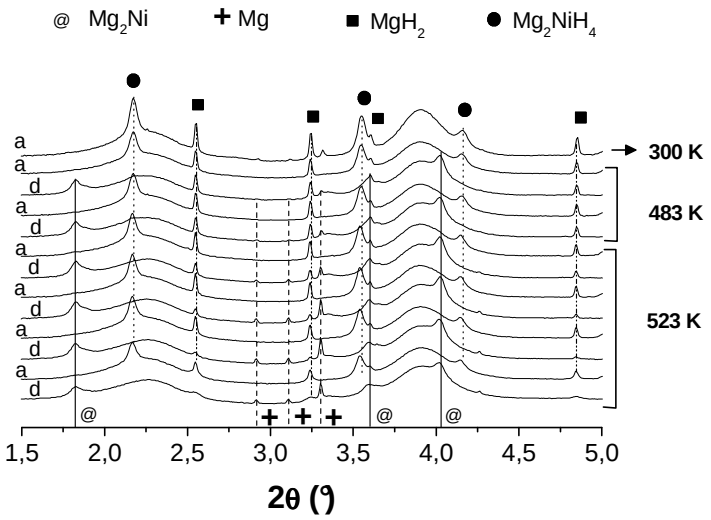

Figure 6. *In situ* XRD patterns of hydrogenated hybrid during cycling at 523 and 483 K by switching the hydrogen pressure between 0.03 and 0.57 MPa. The symbols *a* and *d* stand for absorption and desorption, respectively. The pattern on top was recorded at 300 K under 0.57 MPa of H_2.

The hydrogen sorption kinetics of Mg_2Ni improves with cycling. The time to complete the reaction decreases from ~17 min for the first cycle to ~5 min for further cycling, regardless the temperature. The

average particle size of Mg_2NiH_4 is constant at 10 nm upon cycling, whereas that of MgH_2 increases up to around 200 nm.

The cycled sample (containing both Mg_2NiH_4 and MgH_2 crystalline phases at room temperature) was analyzed by TEM (Figure 7).

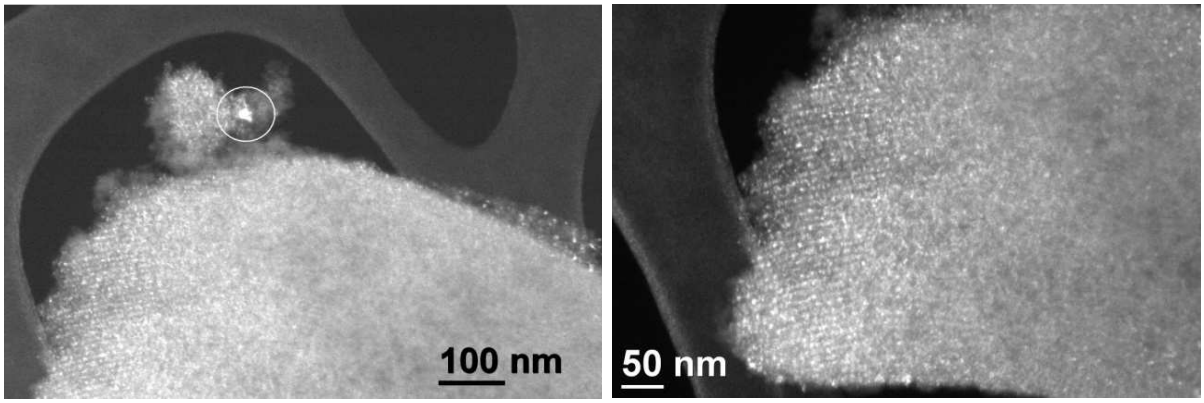

Figure 7. Dark field TEM image of cycled hybrid.

The dark field images clearly show small nanoparticles well dispersed within the CT as well as larger nanoparticles (white circle in Figure 7). The average size of the small nanoparticles is approximately 4 nm, as determined by TEM analysis.

The hydrogen sorption properties of as-synthesized (crystalline phases: MgH_2 + Ni) and hydrogenated (0.57 MPa of H_2 and 523 K; crystalline phases: MgH_2 + Mg_2NiH_4) hybrids have been studied by TDS and DSC measurements.

Figure 8 shows the hydrogen TDS spectra of as-synthesized and hydrogenated samples recorded with a temperature ramp of 10 $K \cdot min^{-1}$. Only one broad desorption peak with a maximum at 600 K is observed for the as-synthesized sample whereas the hydrogenated sample exhibits two narrower peaks with maxima located at 460 and 580 K.

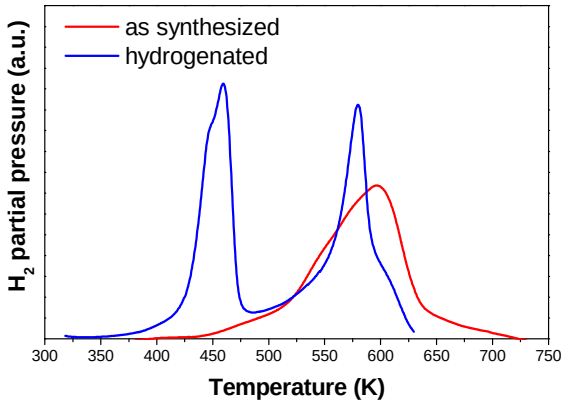

Figure 8. TDS spectra of the as-synthesized and hydrogenated hybrids (temperature rate 10 K·min^{-1}).

DSC measurements were performed on the as-synthesized and hydrogenated samples by heating up to 670 K at 5 K·min^{-1} (Figure 9). The as-synthesized sample was measured under high (2 MPa) and low (< 0.1 MPa) H_2 pressure. The hydrogenated sample was measured under low H_2 pressure only (< 0.1 MPa).

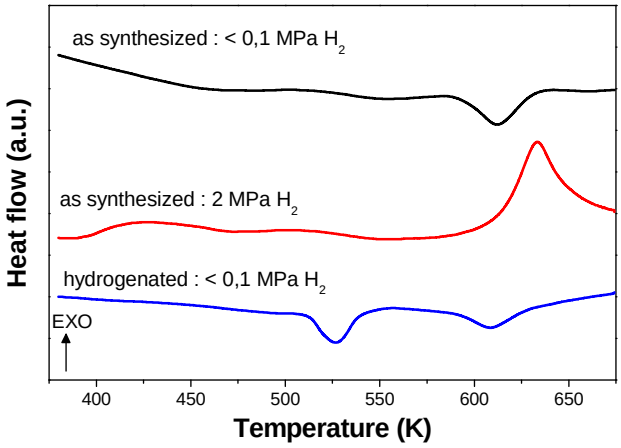

Figure 9. DSC measurements of the as-synthesized and hydrogenated hybrid under different hydrogen pressures with a temperature ramp of 5 K·min^{-1}.

The as-synthesized shows an endothermic peak at 612 K at low H_2 pressure (black curve) and an exothermic peak at 633 K under high pressure (red curve). Two endothermic peaks at 527 and 609 K are noticed for the hydrogenated sample (blue curve).

4. Discussion

a. Synthetic reactions

The as-synthesized hybrid was prepared in two steps: firstly, Ni nanoparticles were formed into the CT pores and secondly, MgH_2 nanoparticles were added. TEM images clearly prove that both Ni and MgH_2 nanoparticles are homogeneously distributed inside the porosity of CT (Figure 1). However, formation of nanoparticles at the external surface of the CT cannot be excluded. The nanoparticles sizes range between 2 and 10 nm, whatever the nature of nanoparticles.

The reactivity of these crystalline phases has been studied by *in situ* synchrotron XRD (Figures 2 and 3) under different H_2 pressure and a constant temperature ramp (2 $K \cdot min^{-1}$). Both Ni (cubic $Fm\bar{3}m$) and MgH_2 (tetragonal $P4_2/mnm$) crystalline phases are initially present. The *in situ* study demonstrates that Ni and MgH_2 nanoparticles start to react at 570 K to form either the Mg_2Ni phase (Figure 2) or the Mg_2NiH_4 hydride (Figure 3), depending on the applied H_2 pressure and in agreement with the equilibrium pressure expected for the system Mg_2Ni/Mg_2NiH_4 at this temperature. The reaction pathway under 0.56 MPa H_2 pressure is illustrated in Figure 2 and Equation 1.

$$Ni + (2+x)MgH_2 \rightarrow Mg_2Ni + xMg + (2+x)H_2 \uparrow \quad \text{(Equation 1)}$$

where *x* stands for the excess amount of Mg to that needed for the synthesis of stoichiometric Mg_2Ni. The temperature domain for this reaction spans between 570 and 620 K. Starting from 570 K, both Ni and MgH_2 amounts decrease and Mg_2Ni is formed (Figure 2 - right). Two possible intermediate mechanisms may account for this reaction: either MgH_2 desorbs hydrogen forming Mg that directly reacts with Ni to produce Mg_2Ni or MgH_2 reacts with Ni forming Mg_2NiH_4, which is unstable under these conditions and instantly desorbs hydrogen by forming Mg_2Ni. The intermediate reactions occur simultaneously and no experimental evidence was found to discriminate between these two possible mechanisms.

Under 2 MPa of H_2 pressure, the reaction pathway can be summarized by Equation 2 according to Figure 3.

$$Ni + (2+x)MgH_2 \rightarrow Mg_2NiH_4 + xMgH_2 \quad \text{(Equation 2)}$$

This reaction begins at 570 K when, both Ni and MgH_2 phases start to vanish simultaneously forming directly the Mg_2NiH_4 hydride (cubic $Fm\bar{3}m$). This reaction is a solid/solid reaction and stops when all Ni is consumed. The final sample contains both Mg_2NiH_4 and MgH_2 hydrides.

DSC measurements confirm that the as-synthesized hybrid reacts differently depending on the applied H_2 pressure (Figure 9). At low pressure, only one endothermic peak is noticed at 612 K. As stated before, two possible intermediate mechanisms may explain the formation of Mg_2Ni from initial MgH_2 and Ni. These intermediate reactions occur simultaneously therefore, a clear explanation of the unique endothermic peak is not straightforward. Moreover, the heats of endothermic desorption of MgH_2 (-74 $kJ \cdot mol^{-1}$ H_2)[17] and Mg_2NiH_4 (-64 $kJ \cdot mol^{-1}$ H_2)[18] are much larger than that of exothermic Mg_2Ni formation (-13 $kJ \cdot mol^{-1}$)[19]. Consequently, an endothermic feature is expected to be observed, whatever the intermediate pathway.

On the contrary, under higher H_2 pressure, an exothermic peak is observed at 633 K, without any endothermic peak that might suggest hydrogen desorption from MgH_2. This corroborates with our proposed mechanism for a solid/solid reaction between MgH_2 and Ni to form Mg_2NiH_4 hydride under higher H_2 pressure (Equation 2). However, the DSC reaction temperature range (600 – 660 K) is slightly higher that the *in situ* XRD (570 – 630 K) but such temperature shift is not surprising when switching from one instrument and technique to another.

To produce stoichiometric bulky Mg_2NiH_4 hydride, the common method is the hydrogenation of the intermetallic compound Mg_2Ni. The latter one can be prepared at high temperature by many different method such as induction melting[18], mechanical alloying[20], combustion synthesis[21] or melt spinning[22]. Owing to slow kinetics at moderate temperature, all publications report hydrogenation at high temperature (473 - 623 K).[23] Reactive ball milling (under H_2 gas pressure) can also be used to prepare the hydride Mg_2NiH_4 from pure elements.[24,25] Starting from Mg and Ni nanoparticles, Shao et al. synthesized the Mg_2Ni phase by heating under different gas atmospheres[26]. Mg_2Ni phase was obtained from Mg (500 nm) and Ni (30 nm) nanoparticles under 3 MPa of H_2 pressure at 553 K, which is in

disagreement with our findings and the thermodynamic properties of Mg_2NiH_4. At 570 K and 2 MPa H_2 pressure, our results show the direct formation of Mg_2NiH_4 hydride.

To our knowledge, this is the first report on the formation at moderate temperature of either intermetallic Mg_2Ni compound or complex Mg_2NiH_4 hydride starting from separate Ni and MgH_2 nanoparticles by tuning the H_2 pressure. At low pressure (< 0.5 MPa), the intermetallic Mg_2Ni phase is formed. At high pressure (2 MPa), the hydride Mg_2NiH_4 phase is synthesized through a single solid-solid reaction.

b. Pressure-composition-isotherm at 523 K

The desorption PCT curve of nanosized Mg_2NiH_4 derived from XRD analysis at 523 K (Figure 5 - right) shows a sloppy plateau pressure between 0.07 and 0.1 MPa typical for metallic nanoparticles.[8,27] The plateau domain is in good agreement with the desorption plateau pressure of bulk Mg_2NiH_4 at this temperature (0.09 MPa at 523 K).[18] This indicates that the thermodynamic properties of nanoconfined Mg_2NiH_4 are preserved. This not surprising since modification of the thermodynamic properties is predicted by theory for particles smaller than 2 nm in the closely related Mg-H system.[28]

c. Cycling behavior

Six desorption/absorption cycles of hydrogenated hybrid have been performed at 523 K and 483 K by varying the gas pressure between 0.03 and 0.57 MPa (Figure 6). The desorption/absorption in Mg_2NiH_4 is completely reversible under these conditions, whatever the temperature. Moreover, the hydrogen sorption kinetics improve by cycling. The complete reaction occurs in ~17 min for the first cycle and decreases to ~5 min for further cycling, regardless the temperature.

The hydrogenated sample was finally cooled down to 300 K under 0.57 MPa (Figure 6 - top). Is it known that bulk Mg_2NiH_4 undergoes an polymorphic phase transition at 510 K from a cubic high temperature structure (HT) to a monoclinic distorted low temperature modification (LT).[29] Surprisingly, nanosized Mg_2NiH_4 (~4 nm by TEM analysis) does not show any phase transition upon cooling and preserves the HT cubic structure at room temperature. Previous studies on bulk Mg_2NiH_4 (LT) have established that the compression under 1.3 to 2.0 GPa induces the transformation from LT structure into

the pseudo-cubic HT form at room temperature.[30,31] This similarity suggests a nanosized / nanoconfined effect in the Mg_2NiH_4 hydride. At nanoscale, thermodynamic description must take into account the interfacial energy or surface energy that contributes as an induced additional pressure increasingly important with decreasing the particle size.[32] This effect has been quantified for carbon phase diagram at nanoscale and predicts, for example, an additional pressure of 2 GPa for nanocrystals with 4 nm radius.[33] To our knowledge, this is the first report of a nanosized induced effect on the structural properties of a Mg-based hydride.

d. Particle size variation

The particle size thermal variation upon heating under 2 MPa (Figure 4) provides evidence of different behaviors between Mg_2NiH_4 and MgH_2 phases. The latter one preserves a constant particle size (~ 8 nm) up to 570 K but it steadily increases above this temperature reaching 200 nm at 660 K. In contrast, the particle size of Mg_2NiH_4 at 570 K is constant (~10 nm) over the whole temperature domain. Pure Mg nanoparticles also easily agglomerates as observed during both low H_2 pressure measurement (first *in situ* XRD experiment) and hydrogenation/dehydrogenation cycling experiments at 523 K (fourth *in situ* XRD experiment). Moreover, *ex situ* TEM images after cycling (Figure 7) clearly show small nanoparticles well dispersed within the CT as well as the presence of larger nanoparticles. The latter can be unambiguously attributed to the MgH_2 phase and the small ones to Mg_2NiH_4, as proven by *in situ* XRD. TEM analysis demonstrates that the average size of Mg_2NiH_4 is ~4 nm after cycling. This value is two times lower than the one obtained from XRD (~10 nm). This discrepancy might come from the XRD particle size analysis. Consistent results are obtained by direct TEM observation.

The average size of Mg_2NiH_4 nanoparticles is 4 nm, which is in very good agreement with the mean pore size of the CT host, proving an effective nanoconfinement of Mg_2NiH_4.

Obviously, the coalescence of nanoparticles occurs very easily for Mg/MgH_2, whereas Mg_2Ni/Mg_2NiH_4 nanoparticles are stable upon prolonged exposure to high temperature and hydrogenation/dehydrogenation cycling. This proves that Mg/MgH_2 has a significant mobility at high temperature, whereas it possesses lower diffusivity when alloyed with heavier metal such as, Ni. This

may be understood in term of weight of involved elements, since the diffusion rate is proportional to the square of inversed mass of species. The high mobility of Mg/MgH_2 might also explain the high reactivity with Ni forming either Mg_2Ni or Mg_2NiH_4 phases.

Generally, Mg-based nanoparticles agglomerate during cycling and heating at high temperature, which worsen the hydrogen sorption properties.[34] Therefore, stabilization of Mg-based nanoparticles by nanoconfinement is compulsory for an efficient storage device. However, reports on the stability of nanoconfined particles against coalescence are very scarce. In this context, the present results are very promising and provide evidences for an effective nanoconfinement of Mg_2NiH_4 within the CT with a very good stability during cycling and exposure to high temperature.

e. Hydrogen desorption properties

The as-synthesized sample contains a mixture of Ni and MgH_2 nanoparticles showing one single desorption peak in the TDS spectrum (Figure 8) that corresponds to the dissociation of MgH_2. The peak shape and the maximum temperature of the desorption rate (~600 K) are in agreement with our previous results obtained on MgH_2 nanoparticles embedded into CT.[15]

The hydrogenated hybrid (0.57 MPa, 523 K) contains two hydrides Mg_2NiH_4 and MgH_2. Consequently, two peaks are noticed in the TDS spectrum with maxima at 460 and 580 K corresponding to desorption from Mg_2NiH_4 and MgH_2, respectively. DSC measurement on the hydrogenated sample confirms the two-step desorption though two endothermic maxima. These peaks are slightly shifted to higher temperature (527 and 609 K) as compared to TDS measurement (460 and 580 K). This discrepancy might be explained by different temperature ramp (10 $K \cdot min^{-1}$ for TDS and 5 $K \cdot min^{-1}$for DSC) and environment (high vacuum and low hydrogen pressure for TDS and DSC, respectively).

The TDS desorption peak from our nanosized Mg_2NiH_4 occurs at lower temperature (460 K) than bulk Mg_2NiH_4 (500 K, 5 $K \cdot min^{-1}$)[35] or $Mg_{1-x}Ni_xH_y$ nanocrystals (10-30 nm) supported on carbon (~500 K , 5 $K \cdot min^{-1}$)[10]. This clearly points out an enhancement of the desorption kinetics of Mg_2NiH_4 by nanoconfinement into the mesopores of CT. Moreover, the hydrogen desorption of MgH_2 takes place at 580 K, which is lower temperature than the as-synthesized sample. A cooperative effect of Mg_2NiH_4

might explain the faster desorption from MgH_2, despite the coalescence of MgH_2 nanoparticles by exposure to high temperature during cycling.

5. Conclusions

Starting from individual Ni and MgH_2 nanoparticles, this study reports on the formation of either intermetallic Mg_2Ni or complex Mg_2NiH_4 hydride by tuning the H_2 pressure at moderate temperature. At low pressure (< 0.5 MPa), the intermetallic Mg_2Ni phase is formed. At high pressure (2 MPa), the stoichiometric Mg_2NiH_4 hydride is synthesized in a single step from the initial MgH_2 and Ni nanoparticles.

The average particle size is around 4 nm for both Mg_2Ni and Mg_2NiH_4 nanoparticles, whereas the Mg and MgH_2 nanoparticles coalesce into large aggregates up to 200 nm at high temperature. This result proves a higher mobility of Mg/MgH_2 species as compared to Mg_2Ni/ Mg_2NiH_4.

The polymorphic transition from cubic HT to monoclinic LT structures is suppressed in Mg_2NiH_4, which remains in the HT cubic structure at 300 K. This is the first report of a nanosized and/or nanoconfinement effect on the crystalline structure of Mg_2NiH_4.

Hydrogen absorption/desorption in nanoconfined Mg_2Ni is reversible and proceeds rapidly even at 483 K (~ 5min). The hydrogen desorption kinetics from nanosized Mg_2NiH_4 is enhanced as compared to other $Mg_{1-x}Ni_xH_y$ nanocrystals supported on carbon.

Both Mg_2Ni and Mg_2NiH_4 nanoparticles are extremely stable against coalescence during sorption cycling and exposure to high temperature confirming a successful nanoconfinement into the pores of CT. Moreover, the average size of these nanoparticles corresponds exactly to the pore size of templated carbon host. These results open a promising route for effective nanoconfinement of complex metallic hydrides within the porosity of carbon nanostructures.

ACKNOWLEDGMENTS

The authors are thankful to Diana Dragoe for ICP-OES, Benjamin Villeroy and Valérie Lalanne for DSC measurements.

REFERENCES

1. P.E. de Jongh and P. Adelhelm, *Chemsuschem*, 2010, **3**, 1332-1348.
2. M. Fichtner, *Physical Chemistry Chemical Physics*, 2011, **13**, 21186-21195.
3. U. Eberle, M. Felderhoff and F. Schuth, *Angewandte Chemie-International Edition*, 2009, **48**, 6608-6630.
4. S. Zhang, *et al.*, *Nanotechnology*, 2009, **20**.
5. J.J. Vajo, *Current Opinion in Solid State and Materials Science*, 2011, **15**, 52-61.
6. T.K. Nielsen, *et al.*, *ACS Nano*, 2009, **3**, 3521-3528.
7. M. Paskevicius, *et al.*, *Journal of Physical Chemistry C*, 2011, **115**, 1757-1766.
8. C. Zlotea, *et al.*, *Journal of the American Chemical Society*, 2010, **132**, 7720-7729.
9. Z. Zhao-Karger, *et al.*, *Chemical Communications*, 2010, **46**, 8353-8355.
10. R. Bogerd, *et al.*, *Nanotechnology*, 2009, **20**.
11. R. Ryoo, S.H. Joo and S. Jun, *The Journal of Physical Chemistry B*, 1999, **103**, 7743-7746.
12. C. Vix-Guterl, *et al.*, *Chemistry Letters*, 2002, 1062-1063.
13. F. Ehrburger-Dolle, *et al.*, *Langmuir*, 2003, **19**, 4303-4308.
14. R. Campesi, *et al.*, *Microporous and Mesoporous Materials*, 2009, **117**, 511-514.
15. C. Zlotea, *et al.*, *Faraday Discussions*, 2011, **151**, 117-131.
16. J.R. Ares, F. Cuevas and A. Percheron-Guegan, *Acta Materialia*, 2005, **53**, 2157-2167.
17. P. Selvam, *et al.*, *International Journal of Hydrogen Energy*, 1986, **11**, 169-192.
18. J.J. Reilly and R.H. Wiswall, *Inorganic Chemistry*, 1968, **7**, 2254-2256.
19. de Boer F. R., *et al.*, *Cohesion in Metals: Transition Metal Alloys*, ed. P.D. de Boer FR. 1989: North Holland.
20. M.Y. Song, *International Journal of Hydrogen Energy*, 1995, **20**, 221-227.
21. T. Akiyama, H. Isogai and J.-i. Yagi, *Powder Technology*, 1998, **95**, 175-181.
22. T. Spassov and U. Kaster, *Journal of Alloys and Compounds*, 1999, **287**, 243-250.
23. J. Cermak, L. Kral and B. David, *Intermetallics*, 2008, **16**, 508-517.
24. A. Zaluska, L. Zaluski and J.O. Ström-Olsen, *Journal of Alloys and Compounds*, 1999, **289**, 197-206.
25. J.X. Zhang, *et al.*, *Journal of Physical Chemistry C*, 2010, **115**, 4971-4979.
26. H. Shao, *et al.*, *Scripta Materialia*, 2003, **49**, 595-599.
27. A. Pundt and R. Kirchheim, *Annual Review of Materials Research*, 2006, **36**, 555-608.
28. R.W.P. Wagemans, *et al.*, *Journal of the American Chemical Society*, 2005, **127**, 16675-16680.
29. Z. Gavra, *et al.*, *Inorganic Chemistry*, 1979, **18**, 3595-3597.
30. S. Yamamoto, *et al.*, *Journal of Alloys and Compounds*, 2003, **356-357**, 697-700.
31. E. Rönnebro, *et al.*, *Journal of Alloys and Compounds*, 2004, **385**, 276-282.
32. C.X. Wang and G.W. Yang, *Materials Science and Engineering: R: Reports*, 2005, **49**, 157-202.
33. C.Y. Zhang, *et al.*, *The Journal of Physical Chemistry B*, 2004, **108**, 2589-2593.
34. O. Friedrichs, *et al.*, *Acta Materialia*, 2006, **54**, 105-110.
35. H. Itoh, O. Yoshinari and K. Tanaka, *Journal of Alloys and Compounds*, 1995, **231**, 483-487.